PROBING THE "30 μm" FEATURE: LESSONS FROM EXTREME CARBON STARS

Citation: Messenger, Stephen J., Angela Speck, and Kevin Volk. "PROBING THE '30 Mm' FEATURE: LESSONS FROM EXTREME CARBON STARS." The Astrophysical Journal 764, no. 2 (February 1, 2013): 142. © 2013 The American Astronomical Society

As Published: http://dx.doi.org/10.1088/0004-637x/764/2/142

Publisher: IOP Publishing

Persistent URL: http://hdl.handle.net/1721.1/94540

Version: Final published version: final published article, as it appeared in a journal, conference proceedings, or other formally published context

The Astrophysical Journal, 764:142 (15pp), 2013 February 20 doi:10.1088/0004-637X/764/2/142

PROBING THE "30 μm" FEATURE: LESSONS FROM EXTREME CARBON STARS

Stephen J. Messenger[1], Angela Speck[2], and Kevin Volk[3]
[1] Massachusetts Institute of Technology, 77 Massachusetts Avenue, 54-1717 Cambridge, MA 02139, USA; sjm7w6@mit.edu
[2] 223 Physics, University of Missouri, Columbia, MO 65211, USA; speckan@missouri.edu
[3] Space Telescope Science Institute, 3700 San Martin Drive, Baltimore, MD 21218, USA; volk@stsci.edu
Received 2011 October 24; accepted 2012 December 19; published 2013 February 1

ABSTRACT

Some carbon-rich evolved stars exhibit a very prominent spectral feature at ~"30 μm." The C-rich nature of these objects suggests that the carrier is a sulfide, carbide, or other substance apt to form in a reducing environment. However, the carrier of this spectral feature remains disputed, with magnesium sulfide (MgS) as the most favored candidate. In order to investigate the carrier of the "30 μm" feature further, we have taken a dual approach, studying both laboratory and observational data. In order to obtain a homogeneous sample, we studied the "30 μm" feature observed in the spectra of galactic extreme carbon stars that exhibit the 11 μm SiC absorption feature. Thus, we avoid potential differences in the target objects that could contribute to the observed differences in the shape, position, and strength of the "30 μm" feature. In addition, we analyzed the shape and position of the "30 μm" features for a range of sulfide minerals for which laboratory data exist. Our study of observed astronomical features shows a range of shapes and positions for the "30 μm" feature despite similarities in the source objects. The nature of our sample argues against grain processing or temperature differences due to hardening of the stellar radiation field with evolution. While there are very few correlations between spectral parameters for our sample, the peak positions of the ~11 μm absorption and 30 μm emission features do correlate, and these peak positions correlate with the modeled optical depth. These correlations suggest that the carriers of the observable spectral features are closely related to one another and to the density/pressure in the dust formation zone. Furthermore, we suggest that the blue-broadening of the 11 μm feature cannot be attributed to SiS_2 based on existing laboratory spectra, but further lab work is needed to investigate the effect of increasing oxidation.

Key words: circumstellar matter – dust, extinction – infrared: stars – stars: AGB and post-AGB – stars: carbon

1. INTRODUCTION

1.1. Physical and Chemical Evolution of Intermediate-mass Stars and Their Circumstellar Shells

Stars between about 1 and 8 $M_\odot$ eventually evolve up the asymptotic giant branch (AGB; Iben & Renzini 1983). Because of instabilities in their interior, AGB stars pulsate and throw off large amounts of mass from their surface (e.g., Vassiliadis & Wood 1993). This intensive mass loss produces a circumstellar shell of dust and neutral gas. Once the AGB star has exhausted its outer envelope, the AGB phase ends. At this point, the mass loss virtually stops and the circumstellar shell moves away from the star. At the same time, the central star begins to shrink and heat up from ~3000 K until it is hot enough to ionize the surrounding gas, at which point the object becomes a planetary nebula (PN). Toward the end of the AGB phase, the increasing impact of the thermal pulse cycles leads to an enhanced mass-loss rate (e.g., Vassiliadis & Wood 1993; Villaver et al. 2002a). Such an increase in mass-loss rate (dubbed the *superwind*) is necessary to explain the densities seen in typical PNe (Renzini 1981). Since the initial suggestion of the superwind hypothesis, many observations of AGB and post-AGB stars have supported this hypothesis (e.g., Knapp & Morris 1985; Wood et al. 1992).

The chemical composition of the atmospheres of AGB stars is expected to change as these stars evolve, due to convective dredge up of carbon produced in the He-burning shell. The carbon-to-oxygen ratio (C/O) is critical in determining which types of dust and molecules are present around an AGB star. The formation of extremely stable CO molecules will consume almost all of the less abundant element, leaving only the more abundant element available for dust formation. Stars start their lives with the cosmic C/O of ≈0.4 and are therefore oxygen-rich. In about one-third of AGB stars, enough carbon will be dredged up to make C/O > 1, and, therefore, carbon will dominate the chemistry around these stars, known as carbon stars. If carbon stars reach the optically obscured superwind phase, they become known as "extreme carbon stars" (Volk et al. 1992). See Speck et al. (2009) for a review of extreme carbon stars and their dust.

1.2. Dust Around Carbon Stars

Carbon stars are expected to have circumstellar shells dominated by amorphous or graphitic carbon grains. Unfortunately, these carbon-only grains do not have diagnostic infrared (IR) spectral features. Other predicted components of the dust shells include various carbide, nitride, and sulfide grains (see Speck et al. 2009 and references therein for a review of observed and hypothetical condensates around carbon stars).

The most important dust component after "pure" carbon grains is silicon carbide (SiC), which has an IR spectral feature at ≈11 μm. SiC was long predicted to be present in carbon star circumstellar shells, beginning with theoretical condensation models (Friedman 1969; Gilman 1969) and continuing with the prediction of a characteristic ~11 μm spectral feature (Gilra & Code 1971). The observational discovery of an ~11 μm emission feature in many carbon star spectra (Hackwell 1972; Treffers & Cohen 1974) provided a means to study dust around carbon stars.

There have been numerous studies of the ~11 μm feature in carbon star spectra, and several focused on how the shape and position of the feature vary from object to object (Cohen

1984; Baron et al. 1987; Willems 1988; Chan & Kwok 1990; Goebel et al. 1995; Speck et al. 1997, 2005, 2006, 2009; Sloan et al. 1998; Thompson et al. 2006). Not all these previous works agree. All studies concur that the increasing optical depth leads to decreasing color temperatures from the stars as the stellar photosphere becomes hidden from view and the dust from which we receive light becomes progressively cooler. At the same time, the ~11 μm feature tends to become weaker (relative to the continuum), more flatly topped (less sharply peaked), and possibly broader.

Several studies of the ~11 μm feature have shown that it is consistent with SiC self-absorption, i.e., absorption by cooler SiC particles located in the outer part of the dust shell, where they can absorb the SiC emission feature produced by warmer SiC closer to the central star (Cohen 1984; Speck et al. 1997, 2005, 2009). Indeed, Speck et al. (1997) showed that every star in their sample whose underlying continuum temperature satisfied $T_{\rm col} < 1200$ K was best fitted by self-absorbed SiC, whether the ~11 μm feature was in net emission or net absorption. As the dust shell reaches extreme optical depths, the ~11 μm feature will eventually be seen in net absorption. Furthermore, the ~11 μm SiC feature is seen to vary from object to object in spectral shape and peak position.

When the ~11 μm SiC feature is in net absorption, the observed features have an even larger range of shapes and positions than do the SiC emission features. In particular, this feature seems to range from a "pure" ~11 μm feature as seen in IRAS 23166+1655 to a much broader, bluer feature (e.g., AFGL 2477; Speck et al. 1997). The cause of the broadening to the blue side of the ~11 μm feature remains unknown but has been attributed to an interstellar silicate absorption contribution (see Speck et al. 1997; Groenewegen 1996), silicon nitride (Si_3N_4; Clément et al. 2005), amorphous SiC (Speck et al. 2005), and C_3 (e.g., Zijlstra et al. 2006; Jørgensen et al. 2000). The Si_3N_4 hypothesis has been shown to be erroneous (Pitman et al. 2006), while the suggestion of amorphous SiC is not supported by evidence from pre-solar grains in meteorites (Pitman et al. 2011 and references therein). Speck et al. (2009) argued against C_3 as the cause of the absorption feature on the short wavelength side of the SiC feature. Another plausible contributor to this "blue-broadening" of the ~11 μm feature may be SiS_2. This substance has been invoked to explain the "30 μm" feature (see below) as well as the equally enigmatic 21 μm feature (see Zhang et al. 2009b and references therein). This idea will be discussed further in Section 4.

The ~11 μm absorption feature is most likely caused by SiC grains. Whether the broadening to the blue side of the feature is due to an extra component in the dust shell, or due to structural changes in the SiC grains remains unknown. Whatever the cause of the ~11 μm feature and its variations in peak position and breadth, these variations in spectral parameters should be manifestations of variations in the physical conditions within the dust shell. A detailed study of the ~11 μm feature was presented by Speck et al. (2009), but they did not compare their results with any study of the longer wavelength features.

In addition to the ~11 μm SiC feature, a very prominent feature often appears at ~30 μm in the spectra of some carbon-rich low- and intermediate-mass evolved stars. This so-called 30 μm feature was discovered in the spectra of carbon-rich AGB stars and PNe (Forrest et al. 1981) and has since been observed and studied in many C-rich evolved stars (e.g., Goebel & Moseley 1985; Nuth et al. 1985; Omont et al. 1995; Begemann et al. 1994; Hony et al. 2002b).

The carrier of this spectral feature remains unknown. The C-rich nature of the objects in which the "30 μm" feature is found suggests that the carrier is a sulfide, carbide, or other substance apt to form in a reducing environment. Several such candidate carrier minerals (e.g., Fe_3C, FeS, and SiS_2) have been eliminated from the pool (Nuth et al. 1985). Nuth et al. (1985) suggested both CaS and MgS as potential condensates but favored MgS over CaS due to three claims involving the spectra of CaS: (1) its absorption peaks at 40 μm (and not around 30 μm), (2) its emission around 24 μm does not rise as quickly as observations, and (3) it should be less abundant around stars than MgS (Nuth et al. 1985). However, Lodders & Fegley (1995) found CaS to condense at a higher temperature than MgS, while Hofmeister et al. (2003) produced new laboratory spectra demonstrating the viability of CaS as a carrier of the "30 μm" feature. MgS remains the most favored candidate carrier for the "30 μm" feature, although it is far from universally accepted. For example, Zhang et al. (2009a) showed that the 30 μm feature in HD 56126 is too strong for MgS to be the carrier, as it would require a much larger abundance of MgS than can realistically be expected (see Section 5 for further discussion).

Early observational studies of the "30 μm" feature relied upon observations from the Kuiper Airborne Observatory (KAO; e.g., Omont et al. 1995). Even the *Infrared Astronomical Satellite* (*IRAS*) Low Resolution Spectrometer (LRS; Olnon et al. 1986) spectra did not probe to long enough wavelengths. However, the advent of higher resolution *Infrared Space Observatory* (*ISO*) Short Wavelength Spectrometer (SWS; de Graauw et al. 1996) with broader wavelength coverage has yielded some interesting results. Early *ISO* SWS studies of the "30 μm" feature suggested that the feature can be resolved into two components peaking at ~26 and ~33 μm (Szczerba et al. 1999) and subsequent studies were predicated on this finding (e.g., Volk et al. 2002; Hony et al. 2002b; Zhukovska & Gail 2008). Interestingly, Volk et al. (2002) used the *ISO* spectra to derive the emissivities for these two features and successfully modeled the full range of variations in feature strengths from AGB stars to PN phases, while Hofmeister et al. (2003) found that the laboratory spectra of MgS could be decomposed into two features. However, Hrivnak et al. (2009) used new data from the *Spitzer Space Telescope* to show that the 30 μm feature is not composed of these two sub-features, but rather it is one single broad feature.

Hony et al. (2002b) investigated the effect of grain shape on spectral features of $Mg_{0.9}Fe_{0.1}S$ (from Begemann et al. 1994) and found that while a continuous distribution of ellipsoids (CDE) gave a reasonable match to the astronomical "30 μm" feature, more narrowly defined shapes (e.g., only spheres, or only prolate spheroids, or only oblate spheroids) did not match. However, they did not use other sulfide minerals in their analysis. Hony & Bouwman (2004) produced radiative transfer models of a variety of C-rich environments using CDE $Mg_{0.9}Fe_{0.1}S$ with some success; however, the laboratory spectra used do not cover the visible/near-IR range, which is needed to correctly model the dust emission. Furthermore, the assumption is made that the dust is essentially MgS without examining other possibilities.

This tendency to assume that the "30 μm" feature is due to MgS persists. Leisenring et al. (2008) suggested that there is observational evidence for MgS forming on the surface of SiC grains already extant around carbon-rich stars, i.e., spectroscopic data show correlation between increasing "30 μm" emission and decreasing SiC emission. This observational study is supported by the theoretical grain condensation models of Zhukovska & Gail (2008). However, the Zhukovska & Gail

Table 1
Sample of Extreme Carbon Stars

IRAS Number	Other Names	R.A.[a] (J2000)	Decl. (J2000)	THT Number	Date of Observation
00210+6221	CGCS 6006	00 23 51.2	+62 38 16.4	40401901	1996 Dec 24
01144+6658	V829 Cas, AFGL 190, CGCS 6017	01 17 51.6	+67 13 55.4	68800128	1997 Oct 3
02408+5458		02 44 25.2	+55 11 15	80002504	1998 Jan 24
03313+6058	CGCS 6061	03 35 30.7	+61 08 47.2	62301907	1997 Jul 31
06582+1507	CGCS 6193	07 01 08.44	+15 03 39.8	71002102	1997 Oct 26
17534−3030	AFGL 5416, CGCS 6690	17 56 33.1	−30 30 47.1	12102004	1996 Mar 17
19548+3035	AFGL 2477, CGCS 6851	21 50 45.0	+53 15 28.0	56100849	1997 May 30
21318+5631	AFGL 5625S, CGCS 6888	21 33 22.98	+56 44 35.0	11101103	1997 Mar 7
22303+5950	CGCS 6906	22 32 12.8	+60 06 04.1	77900836	1998 Jan 2
23166+1655	LL Peg, AFGL 3068, CGCS 6913	23 19 12.39	+17 11 35.4	37900867	1996 Nov 29

Note. [a] Units of right ascension are given in hours, minutes, and seconds; units of declination are degrees, arcminutes, and arcseconds.

(2008) model assumed that the 30 μm feature had two components. Furthermore, both the Zhukovska & Gail (2008) and the Leisenring et al. (2008) studies fail to account for observations of SiC absorption features in extreme carbon stars (see Section 1.2, and Speck et al. 2009; Gruendl et al. 2008 and references therein). Moreover, these studies assume that the reduction in peak-to-continuum ratio for the observed 11 μm feature is due to coating of SiC grains, rather than self-absorption effects (see Speck et al. 2005 and references therein).

In this paper, we investigate the "30 μm" feature in the spectra of extreme (i.e., optically obscured) carbon stars with the goal of determining the carrier of the 30 μm feature and testing the hypotheses for C-rich condensation sequences. In Section 2 we discuss our sample selection and data analysis. In Section 3 we present the results of our analysis of the observed spectral features in extreme carbon star data. In Section 4 we reconsider SiS_2 as a condensate to explain observed spectral parameters. Section 5 investigates a selection of laboratory data on sulfides, while Section 6 compares the laboratory data with our observational sample. The findings are summarized and conclusions drawn in Section 7.

2. SAMPLE SELECTION AND OBSERVATIONS

The "30 μm" feature is observed in a range of carbon-rich evolved stars. The evolution of low- and intermediate-mass stars from optically bright AGB stars through the obscured superwind phase and the short-lived post-AGB, pre-planetary nebula (PPN) phase, to the PN phase is described in Section 1.1. During this evolutionary process, the dusty region around a C-rich evolved star changes, chemically, in optical depth, and in the radiation field to which it is exposed. The "30 μm" feature is observed for objects in all these phases of stellar evolution, and thus the factors governing the observed variations in this feature include chemistry, density, and the radiation field. In order to limit the factors that may lead to spectral variations, we have selected a sample containing all known extreme carbon stars in the Galaxy that exhibit the ∼11 μm SiC feature in absorption as of 2008, discussed in Speck et al. (2009). This sample limits us to stars that are in the superwind phases and, thus, all have relatively high-density outflows and low-energy radiation fields. Furthermore, by including only those objects with SiC absorption features, we can use this feature as a diagnostic. Moreover, the occurrence of the SiC absorption feature suggests that SiC grains are not coated with carbon or MgS (see Section 1.2). The objects were all observed by *ISO* and are listed in Table 1.

The raw *ISO* data were extracted from the *ISO* data archive, and we used the Off-Line Processing (OLP) pipeline, version 10.1. Individual spectral sub-bands were cleaned of glitches (caused by cosmic ray particles) and other bad data sections. Next, they were flat-fielded, sigma-clipped (using the default value $\sigma = 3$), and rebinned to the final spectral resolution ($R = \lambda/\Delta\lambda$), which ranged from 200 to 700, depending on the scanning speed of the SWS grating during the observation (Leech et al. 2003). The final spectra are presented in Figure 1 which contains for each source: the *ISO* SWS data, *IRAS* photometry points, *IRAS* LRS data, and continuum fits (described in Section 3). Please note that the intrinsic variability of AGB stars gives rise to changes in brightness and thus the *ISO* and *IRAS* data are often offset in flux.

3. ANALYSIS

3.1. Continuum Fitting and Parameter Measurements

To analyze the spectral features of our extreme carbon stars, we must first estimate the contribution of the continuum. Following Thompson et al. (2006), we assume that the continuum can be approximated by a blackbody or modified blackbody; i.e., $F(\lambda) \propto B_\lambda(T) \times \lambda^{-\beta}$, where β is the emissivity index. The emissivity index β depends on the size, structure, composition, and temperature of the grains as well as on the optical depth of the dust shell (e.g., Mennella et al. 1998; Koike et al. 1980, 1987, 1995). For an optically thick dust shell, one expects the continuum to be well approximated by a blackbody, while more optically thin dust shells are better fit by $F(\lambda) \propto B_\lambda(T) \times \lambda^{-\beta}$. In the case of carbon stars, the dust content, and thus its continuum, is expected to be dominated by carbon grains (see Section 1.2). For carbon grains, the emissivity law is expected to have $\beta \approx 1$ if the grains are amorphous and $\beta \approx 2$ if the grains are graphitic (Mennella et al. 1998; Koike et al. 1995). A distribution of dust temperatures would be represented by a summation of blackbodies and emissivities which may lead to apparent β-values <1. Theoretically, β-values <1 are considered unphysical when one considers a single grain population; however, such values may occur due to summations of emission curves from a distribution of grain sizes and temperatures. Furthermore, measured values of β in laboratory experiments (e.g., Mennella et al. 1998; Koike et al. 1980) have found amorphous carbon to have β-values <1; Rouleau & Martin (1991) found that amorphous carbon has $\beta \approx 0.8$. Combined infrared and submillimeter observations of carbon-rich post-AGB object CRL 618 show that its spectral energy distribution (SED) has a long

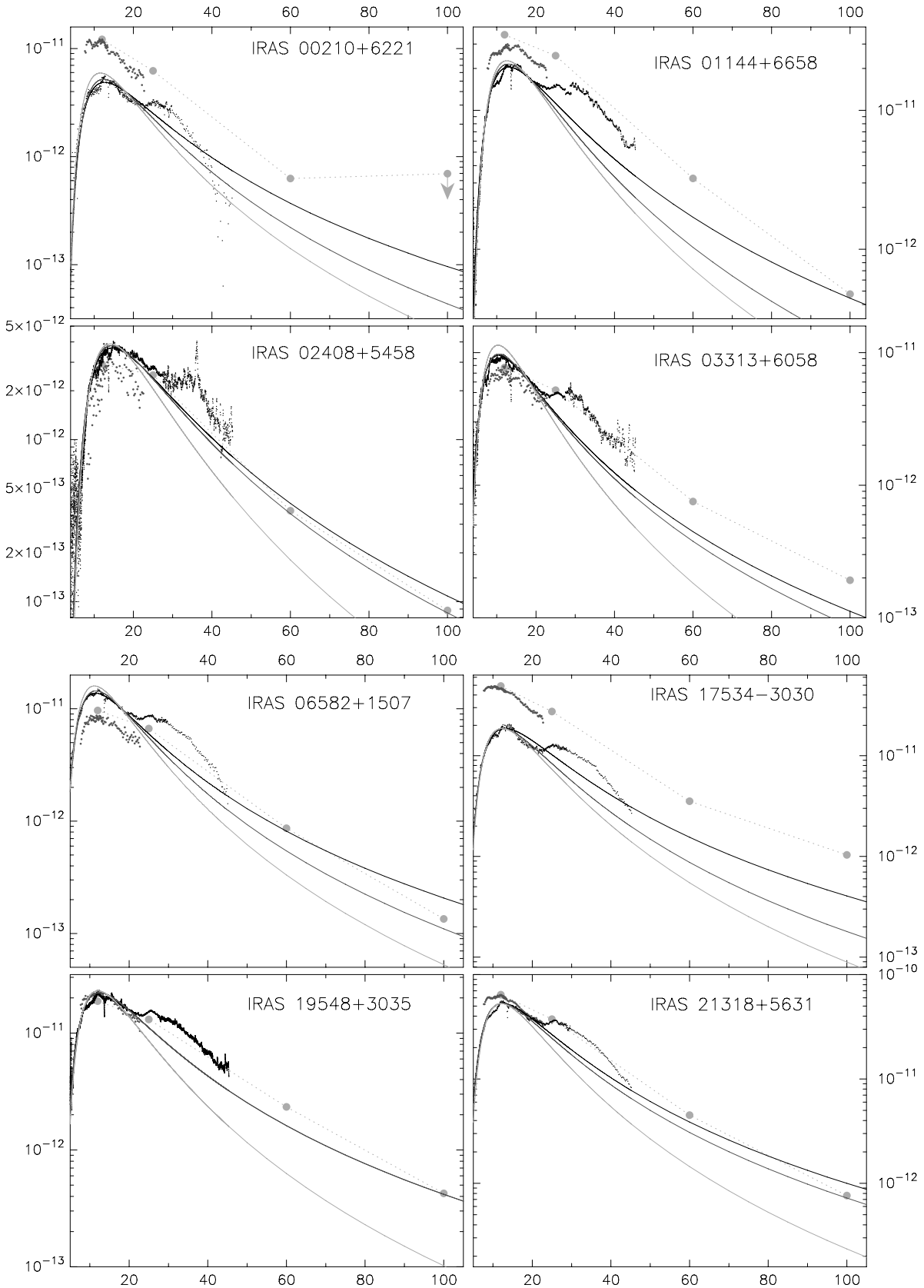

Figure 1. SEDs of our sample of 10 extreme carbon stars. Large dark gray circles are the *IRAS* photometry data, these are connected by a gray dotted line to guide the eye; smaller dark gray circles are the *IRAS* LRS data; black dots are the *ISO* SWS data. Smooth lines indicate the continuum fits: black solid line = pure blackbody ($\beta = 0$); dark gray line = modified blackbody with variable emissivity index; and the light gray line = modified blackbody with $\beta = 1$. The blackbody and modified blackbody temperatures are listed in Table 2. The down arrow indicates an upper limit. The *x*-axis is wavelength in μm and the *y*-axis is flux ($\lambda\ F_\lambda$) in W m^{-2}.

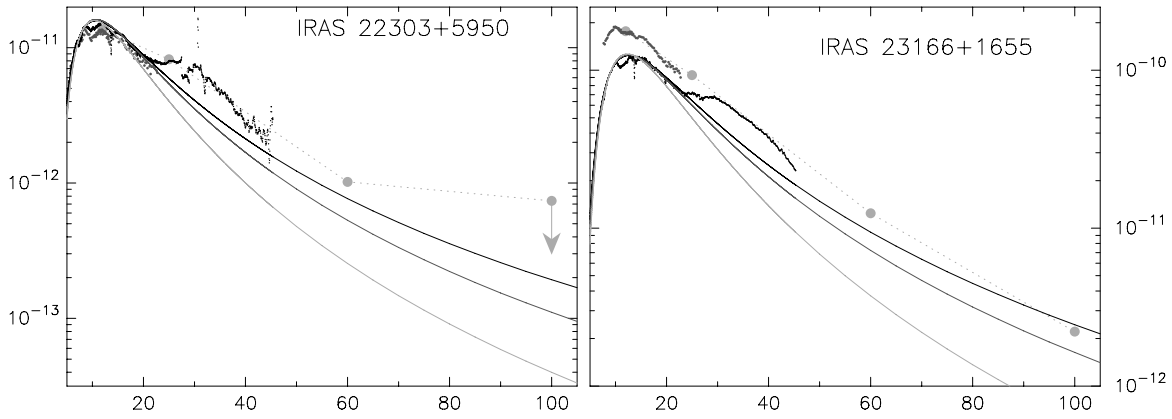

Figure 1. (Continued)

Table 2
Fitted Blackbody and Modified Blackbody Continuum Temperatures and Emissivity Indices

IRAS Name	T_{BB}[a]	T_{BB-Mod}[b] @ $\beta = 1$	T_{BB-Mod}[c] (Best Fit)	β
00210+6621	290	250	255	0.6
01144+6658	280	230	245	0.6
02408+5458	250	205	240	0.2
03313+6058	350	280	330	0.2
06582+1507	320	260	280	0.5
17534−3030	280	235	260	0.6
19548+3035	295	240	295	0.0[d]
21318+5631	295	240	285	0.2
22303+5950	345	280	310	0.4
23166+1655	290	235	270	0.3

Notes. All temperatures are in Kelvin.
[a] T_{BB} is the best-fitting blackbody temperature.
[b] The best-fitting modified blackbody temperature if $\beta = 1$.
[c] The best-fitting modified blackbody temperature if β is allowed to vary.
[d] The best fit is with the blackbody.

wavelength emissivity consistent with $\beta \approx 0.8$ (Knapp et al. 1993). Meanwhile, IRC + 10°216, a carbon-rich AGB star that is not yet completely dust-obscured, has an observed $\beta \approx 1.3$ (Le Bertre 1987). This object is expected to be a precursor to an extreme carbon star and should eventually evolve into a CRL-618-like object. With this in mind, we have fit the continuum for each of our 10 sources 3 times using (1) a blackbody continuum, (2) a modified blackbody continuum for which the emissivity law is set to unity (as expected for amorphous carbon), and (3) a modified blackbody for which the emissivity was allowed to vary to get the best overall fit to the observed SED. For this latter fit, we used the slope of the SED as seen in the *IRAS* photometric observations to guide the steepness of the slope of the fitted continuum. In light of fits to previous laboratory and astronomical data (e.g., Le Bertre 1987; Knapp et al. 1993; Koike et al. 1980), we did not limit the emissivity law to $1 < \beta < 2$. The temperatures and β-values of the fitted continua are listed in Table 2 and the continua are shown in Figure 1.

As seen in Figure 1, the blackbody continua generally overestimate the far-IR continuum, while the steepest continuum ($\beta = 1$) tends to be too steep compared to the *IRAS* SED. It is very important to have an accurate continuum slope because the parameters that define the spectral features in continuum-divided spectra are greatly affected by the choice of continuum.

Having determined three temperature-dependent continua for each spectrum, each one was divided by its assigned continua in order to determine the characteristics of the solid-state spectral features. Continuum-division leaves a temperature-independent emission/absorption efficiency Q_λ, which represents the composite extinction efficiency for all grains in the dust shell. The resulting dust extinction spectra are shown in Figure 2.

For each of the continuum-divided spectra, we determined the parameters of the residual spectral features. Using the NOAO onedspec package within the Image Reduction and Analysis Facility (IRAF), the barycentric position, FWHM, and equivalent width (EW) were determined for the ∼11 μm SiC absorption feature and the 30 μm emission feature. The parameters for each of these features were determined three times, since we have three fitted continua. While we expect that the values for continua with variable β will be most appropriate, the values derived using the $\beta = 0$ and $\beta = 1$ cases provide an estimate of the errors and serve as a double check on any correlations found between spectral parameters.

The onedspec package allows fitting of spectral features with either a Gaussian or Lorentzian profile; we used both. Typically, the Gaussian profile is popular for astronomical spectroscopic applications. However, a Lorentzian profile is appropriate to the study of solid state spectral features when working in frequency space. In fact, the classical model of emission features from solids is the Lorentz model. It is therefore equivocal which profile is best suited to fitting the observed spectral features. Consequently, we tried both potential profiles and found little difference between using Gaussian or using Lorentzian fits in terms of finding correlations between features. We will only consider the Gaussian fits here.

For the ∼11 μm absorption feature, the attribution to SiC is controversial. Only two sources in the sample (IRAS 23166+1655 and IRAS 02408+5458) show an ∼11 μm absorption feature that clearly "peaks" close to 11 μm with the remaining sources having broader features peaking at slightly shorter wavelengths. Speck et al. (2009) discuss this apparent uneven broadening toward the blue side in the SiC feature and attribute it to an extra feature around 10 μm. Regardless of the true cause of the ∼11 μm absorption feature, the parameters of this feature should be indicators of the physical/chemical state of the circumstellar shell and thus can be used as a diagnostic.

The 30 μm feature is not perfectly Gaussian in shape. However, the general shape of the 30 μm feature is more or less the same throughout all of our sources. Therefore, the best-fitting Gaussian parameters are usable when searching for trends. One particular aspect of the 30 μm feature that may pose a problem

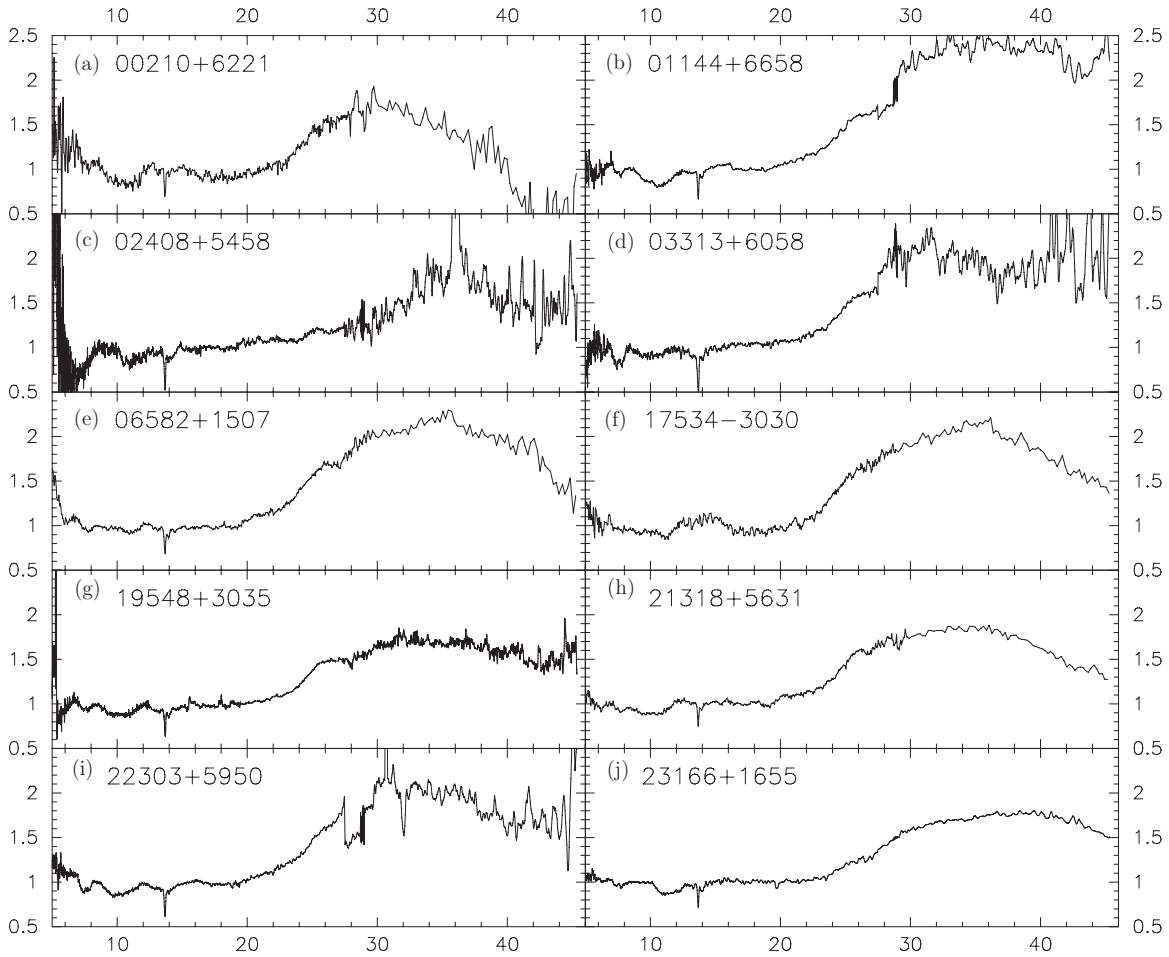

Figure 2. Continuum-divided spectra where continuum is the best-fit modified blackbody (with variable emissivity index) listed in Table 2. The *x*-axis is wavelength in μm and the *y*-axis is emissivity.

in two particular sources, IRAS 03313+6058 and IRAS 19548+3035, is the apparent rise in the flux at longer wavelengths in the *ISO* data. However, these spectra do exhibit a local minimum between the 30 μm and this upward inflection. Hence, our Gaussian fits used the shape up until these minima and do not include the long wavelength rise seen in Figure 1.

3.2. Correlations

Having measured the barycentric position, FWHM, and EW for both spectral features (at 11 and 30 μm), we sought correlations between these parameters and with other spectral parameters (e.g., fitted continuum temperature). In addition, Speck et al. (2009) presented radiative transfer models for each of our sample objects. We used their model parameters for these sources as further potential correlation parameters. In their work, Speck et al. (2009) produced models using, for each source, either the classic "MRN" grain-size distribution[4] or with a larger, but narrower grain-size distribution based on meteoritic pre-solar grains (see Speck et al. 2009; Bernatowicz et al. 2006).

When formally seeking correlations between spectral parameters, it is important to have a suitable measure of the strength of a correlation. We have produced three continua by which our original spectra were divided (β = variable, $\beta = 0$, and $\beta = 1$ cases). While the β = variable case is the best-fitting continuum, we only count a correlation as valid if it occurs regardless of the choice of continuum within the $\beta = 0$ and $\beta = 1$ limits. Furthermore, it is typical in astronomy to define a correlation in terms of the *sample correlation coefficient* (often called "*R*"). This coefficient is usually quoted and there is an implicit assumption that a value of $R \gtrsim 0.5$ constitutes a significant correlation (e.g., Speck et al. 1997; Dijkstra et al. 2005). Thompson et al. (2006) argued that $R = 0.5$ is not sufficient to demonstrate a correlation, but rather that R^2 must be >0.5. Meanwhile, the description of the correlations in Willems (1988) are consistent with either $R > 0.5$ or $R^2 > 0.5$. Dijkstra et al. (2005) used the "*p*-value" to express the significance of finding a correlation but do not discuss what it means. In order to ensure that our analysis is rigorous, it is necessary for us to explain some statistical terms, such as the sample correlation coefficient and coefficient of determination, as well as discuss whether these statistical terms have significance (e.g., see Brockett & Levine 1984; Donnelly 2004). The "*sample correlation coefficient*," *R*, measures both the direction and strength of the relationship between an independent variable *x* and a dependent variable *y*. The value of the sample correlation coefficient is $-1 < R < 1$ such that if $R \sim 0$ there is no relationship between *x* and *y*. The sign (+ or −) of *R* merely designates whether the relationship between *x* and *y* is positive or negative (i.e., it defines the direction of the slope of the trend). It is clear that to choose a value of $R = 0.5$ as a measure of the significance of a correlation is arbitrary.

[4] That is, $n(a) \propto a^{-q}$, where *n* is the number of grains in the size interval $(a, a + da)$ and $q = 3.5$, $a_{\rm min} = 0.005$ μm, and $a_{\rm max} = 0.25$ μm (Mathis et al. 1977).

According to Rumsey (2003), most statisticians like to see $|R| > 0.6$ in order to consider a correlation significant, while Thompson et al. (2006) and Guha-Niyogi et al. (2011) stated that R should be >0.7, in order to be considered a correlation.

Another statistical quantity for correlation studies is the determination coefficient R^2. For a linear-regression fit through a data set, the value of R^2 is a measure of how well the regression line approximates the real data points. If $R^2 = 1.0$, the regression line perfectly fits the data. If $R^2 < 0.5$, then <50% of the data points can be explained by the linear regression fit, i.e., <50% of the variation in y can be attributed to x. Consequently, we use the R^2 value to define a significant correlation and require $R^2 \gtrsim 0.5$. This criterion for significance of correlations is consistent with those used by Thompson et al. (2006), Guha-Niyogi et al. (2011), Xiang et al. (2011), and Greenberg & Chlewicki (1983).

The coefficient of determination for the correlations sought between spectral parameters for the variable-β data are listed in Table 3. Correlated variables ($R^2 \gtrsim 0.5$) are shown in bold face, while the somewhat ambiguous results ($|R| > 0.6 \rightarrow R^2 \gtrsim 0.36$ or not all continua give rise to $R^2 \gtrsim 0.5$) are in italics. The data amongst which the correlations are sought are plotted in Figures 3, 4, 5, and 6. Cross-referencing Table 3 with these figures, we see that the criteria for correlations are valid. For correlations with $0.36 \lesssim R^2 \lesssim 0.5$ (e.g., SiC or 30 μm peak positions with continuum temperature), there is not a discernable trend when the data are plotted.

Although there are correlations (i.e., $R^2 > 0.5$) for several listed pairs of parameters, some of the correlations disappear depending on the choice of continuum. We only consider correlations that exist for all three continuum choices. Figures 3, 4, and 5 show the relationships between the spectral parameters. Both using our statistical criterion of $R^2 > 0.5$ regardless of continuum choice and examining Figures 3, 4, and 5, we can see that there are only two pairs of parameters for which correlations clearly exist: SiC EW versus SiC FWHM, and the barycentric positions for SiC and the ~30 μm feature. In both cases, the correlation exists whether or not the unusual object, IRAS 17534−3030,[5] is included in the correlation assessment. Furthermore, these correlations remain even when we remove extraneous data points or discontinuities within the spectra (see Figures 2(b), (c), and (i)).

Speck et al. (2009) showed that the ~11 μm SiC feature varies significantly in width in such a way that it appears to broaden toward the blue side. This is confirmed by the measurements presented here (see Figure 4 and Table 3). The broadening has been attributed to an extra dust/molecular component in addition to SiC (e.g., interstellar silicate or C_3; see Speck et al. 2009 and references therein). Since the broadening is always to the blue side of the SiC feature, one would expect to find a correlation between the barycentric position and the FWHM of the SiC feature; no such correlation is found. This complicates the interpretation of the feature at ~11 μm and raises the question of whether it is truly due to SiC grains. However, the intrinsic variations in the observed 11 μm emission feature are large and the cause of the variations remains unknown (see Thompson et al. 2006; Speck et al. 2005 and references therein). If the ~11 μm SiC absorption feature were to be similarly variable, this would interfere with finding correlations with the blue component of the absorption feature. We did find a correlation between the FWHM and EW of the SiC feature such that EW scales with the FWHM, suggesting that increasing strength (EW) is largely due to the broadening of the feature.

There is also a correlation between the barycentric positions of both the ~11 μm SiC and the 30 μm features. As the barycentric position of SiC shifts to longer wavelengths, the 30 μm feature also becomes redder. This is true regardless of the choice of continuum with the exception that we do not find such a correlation for the situation where $\beta = 0$ and we include IRAS 17534−3030. In previous work (e.g., Speck et al. 2009; Groenewegen 1996, see also Section 1.2), the ~11 μm feature is assumed to be made up of two superposed features: SiC on the red side and an unknown constituent on the blue side. In this case, the correlation between barycentric position may occur

Table 3
Coefficients of Determination for Correlations between Spectral and Model Parameters

Parameter 1	Parameter 2	R^2
β	T_{BB}	0.2093
β	SiC Center	0.0989
β	SiC EW	0.008
β	SiC FWHM	0.1411
β	30 μm Center	0.0001
β	30 μm EW	0.3057
β	30 μm FWHM	0.1214
β	τ_{met}	0.0516
T_{BB}	*SiC Center*	*0.4102*
T_{BB}	SiC EW	0.0666
T_{BB}	SiC FWHM	0.0489
T_{BB}	*30 μm Center*	*0.3912*
T_{BB}	30 μm EW	0.0287
T_{BB}	30 μm FWHM	2.00E−05
T_{BB}	τ_{met}	0.7871
SiC Center	SiC EW	0.1962
SiC Center	*SiC FWHM*	*0.5727*
SiC Center	**30 μm Center**	**0.5915**
SiC Center	30 μm EW	0.1337
SiC Center	30 μm FWHM	0.0804
SiC Center	τ_{met}	0.2332
SiC EW	**SiC FWHM**	**0.6608**
SiC EW	30 μm Center	0.1081
SiC EW	30 μm EW	0.1079
SiC EW	30 μm FWHM	0.0911
SiC EW	τ_{met}	0.0548
SiC FWHM	30 μm Center	0.2417
SiC FWHM	30 μm EW	0.2627
SiC FWHM	30 μm FWHM	0.0975
SiC FWHM	τ_{met}	0.0118
30 μm Center	30 μm EW	0.001
30 μm Center	30 μm FWHM	0.0002
30 μm Center	τ_{met}	*0.4552 (tentative correlation)*
30 μm EW	*30 μm FWHM*	*0.4855 (tentative correlation)*
30 μm EW	τ_{met}	0.0098
30 μm FWHM	τ_{met}	0.0473

Notes. Listed R^2 values were determined using Gaussian feature shape fits to the β = variable modified blackbody continuum divided spectra. τ_{MRN} and τ_{met} at the modeled optical depths at 10 μm from Speck et al. (2009) for the MRN and meteoritic grain-size distributions, respectively. Bold font indicates where there is a correlation (R^2) regardless of the choice of continuum. The R^2 values are slightly effected by the removal of bad data within IRAS 01144+6658, IRAS 02408+5458, and IRAS 22303+5950. However, for the correlations of interest (bolded) involving the 30 μm feature, the data removal in these cases increased the R^2 values thus strengthening the correlations.

[5] IRAS 17534−3030 does not exhibit the usual strong molecular absorption bands, e.g., C_2H_2 at 13.7 μm. Speck et al. (2009) found that they needed to use unusual parameters in their radiative transfer models for this object.

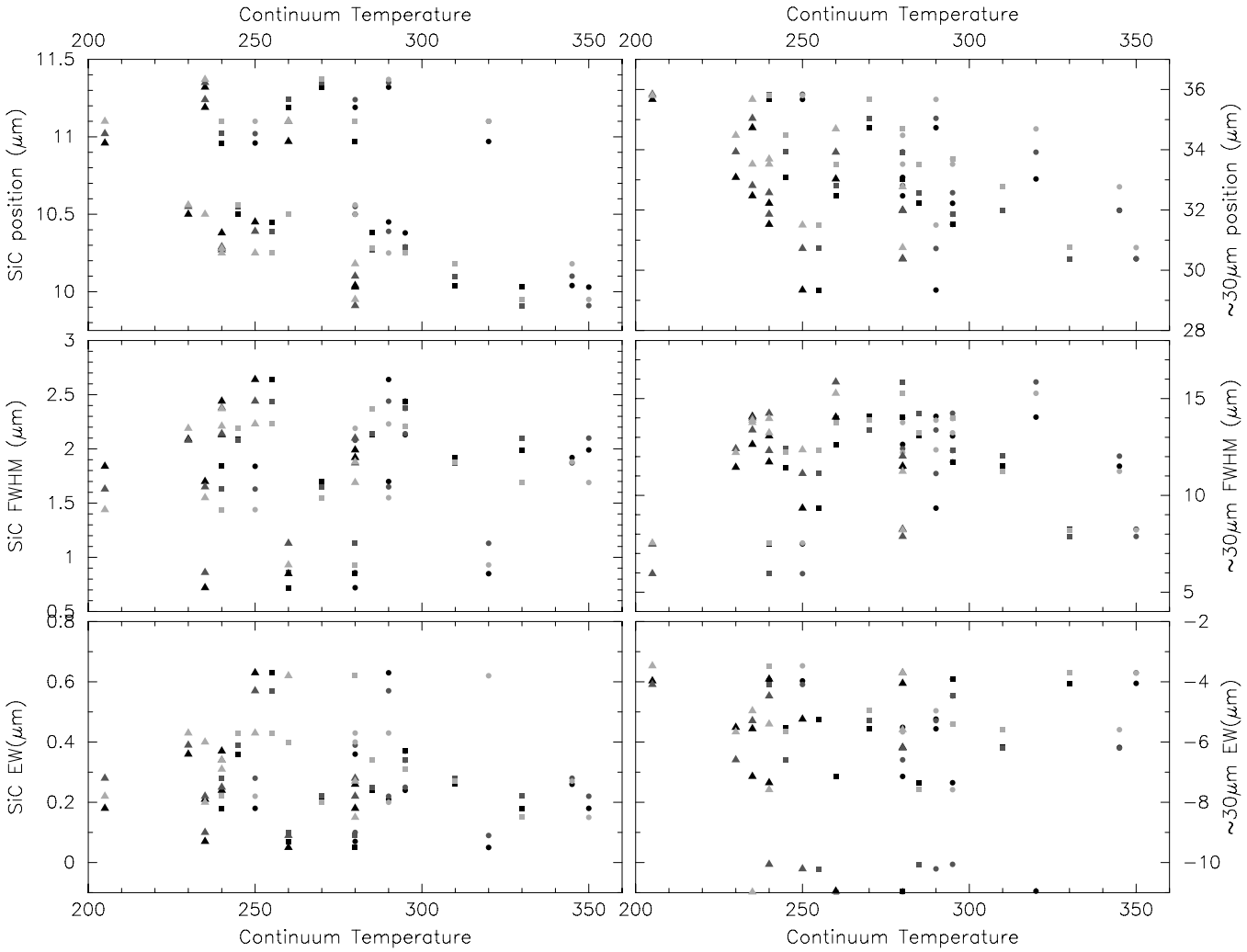

Figure 3. Relationships between continuum temperatures and spectral feature parameters. In all cases, circles are blackbody temperatures; triangles are modified blackbody temperatures with $\beta = 1$; squares are modified blackbody temperatures with best-fit β-value; black symbols are parameters measured on spectra using blackbody continuum division; dark gray symbols are parameters measured on spectra using continuum with best-fit β-value; light gray symbols are parameters measured on spectra using continuum with $\beta = 1$. Upper panels: peak positions; middle panels: FWHMa; lower panels: equivalent widths; left column: values for 11 μm SiC feature; right column: values for "30 μm" feature; the x-axis is always continuum temperature and the y-axis is always in μm.

because the position of the ~30 μm feature is actually correlated with the strength of the unknown constituent on the blue side of the ~11 μm feature. If the unknown constituent were C_3, this may argue for a C/O or C-atom abundance influence on the ~30 μm feature. If the blue constituent is silicate, then C/O may again be important, but the trend would be inverted. Potential causes of this correlation will be discussed further in Section 6. It is worth pointing out that despite our attempt at rigor in defining what constitutes a significant correlation, correlation is not the same as causation. For example, Messerli (2012) showed that there is a strong correlation between a country's per capita chocolate consumption and the number of Nobel prizes it had won. We should be careful when interpreting correlations, even when they are statistically significant.

We do not find a strong correlation (across the choices of continua) between the strengths of the SiC and ~30 μm features. This lack of correlation presents difficulties for previous explanations of the ~30 μm feature which invoke the coating of SiC on MgS dust grains (e.g., Leisenring et al. 2008). If MgS coats SiC grains, one would expect to see an inverse correlation between the SiC and MgS feature strengths (EWs).

We identify two tentative correlations. The barycentric position of the ~30 μm feature apparently increases with the optical depth as found in both the MRN and "meteoritic" radiative transfer models of Speck et al. (2009, see also Figure 6 here). The strength and breadth of the 30 μm feature also appear to have a weak correlation with one another (see Figure 4). For the former, optical depth is really just a measure of the total number of particles in the dust shell. Therefore, the 30 μm feature shifts to longer wavelengths when the dust shell is more densely packed. This may be indicative of a change in the dust species as more dust is created. A denser dust shell may allow for more iron to be included in a sulfide and could naturally explain this correlation. There is not a correlation between the feature wavelength and its strength or breadth, suggesting that the effect is not one of optical depth and self-absorption of the feature, further strengthening the attribution to compositional effects.

Previous research has suggested evolutionary processes to explain the shift in the central peak of the 30 μm feature between different astrophysical sources (Hony et al. 2002b). As a source evolves from an AGB star to a PPN and then, possibly, to a PN, its UV flux increases. It has been suggested that either

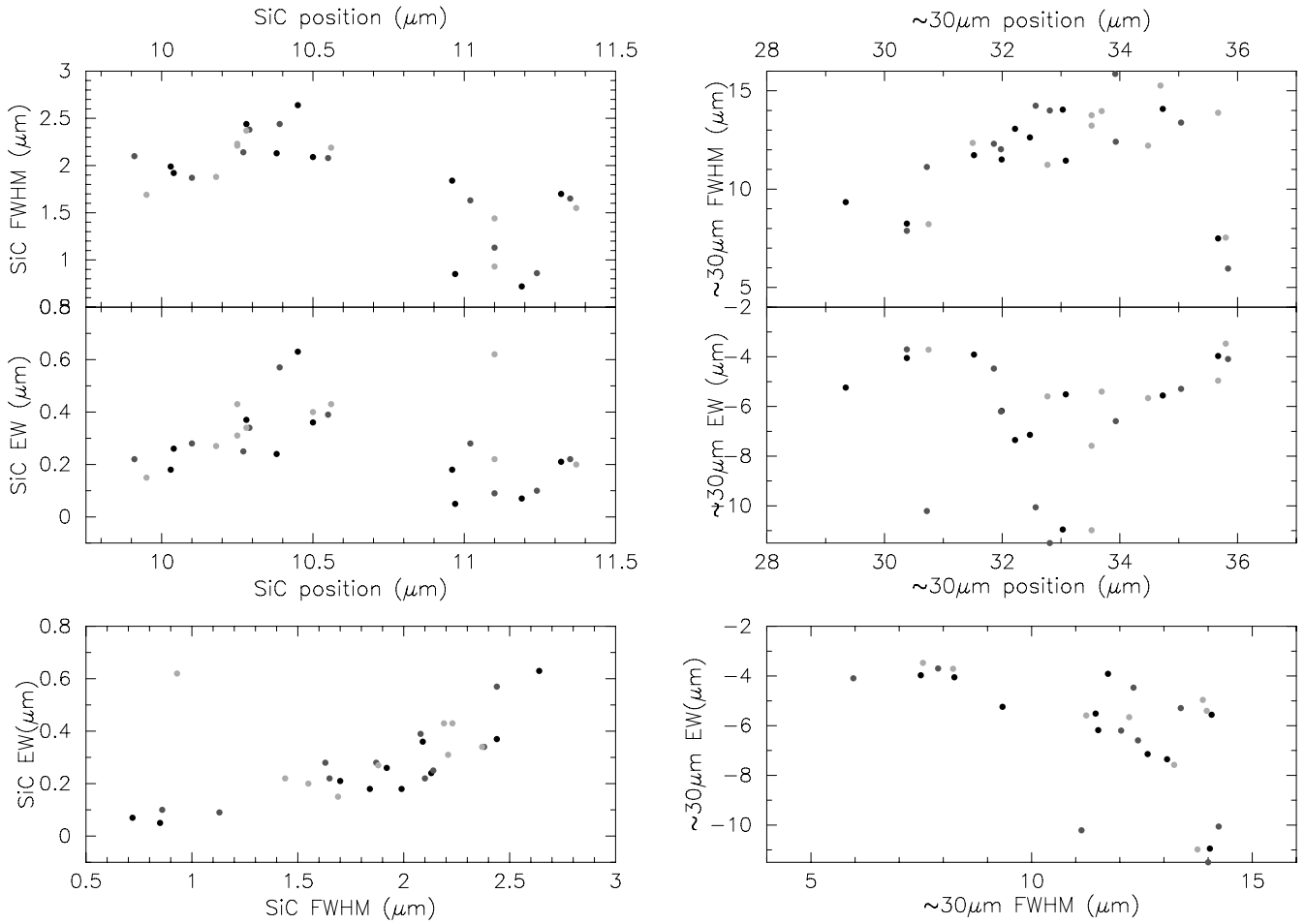

Figure 4. Relationships between spectral feature parameters. In all cases, black symbols are parameters measured on spectra using blackbody continuum division; dark gray symbols are parameters measured on spectra using continuum with best-fit β-value; light gray symbols are parameters measured on spectra using continuum with $\beta = 1$. Upper panels: peak positions vs. FWHM; middle panels: peak positions vs. equivalent widths; lower panels: FWHM vs. equivalent widths; left column: values for 11 μm SiC feature; right column: values for "30 μm" feature; the x- and y-axes are always in μm.

dust temperature or processing due to the harder radiation field gives rise to spectral variations. Here we only present spectra of optically obscured AGB stars so the variations in the 30 μm feature cannot be attributed to changes in the stellar radiation field.

4. SILICON DISULFIDE AND THE BROADENING OF THE 11 μm FEATURE

Silicon disulfide (SiS_2) has been invoked to explain the "30 μm" feature (see Section 1.2) as well as the equally enigmatic 21 μm feature (see Zhang et al. 2009b and references therein).

The spectrum of SiS_2 presented by Kraus et al. (1997) shows that, in addition to an ~21 μm feature, crystalline SiS_2 exhibits a feature at ~9.5 μm attributed to oxygen impurities giving Si–O bonds. This observed feature could potentially contribute to the blue-broadening of the 11 μm feature. Begemann et al. (1996) prepared a glassy SiS_2 sample and took both reflectance and transmission spectra in order to derive the complex refractive index of this substance. Unfortunately, their data do not extend to wavelengths shortward of 12 μm and thus cannot be compared to the blue-broadening of the 11 μm feature. Using absorbance data for SiS_2 from A. M. Hofmeister (2012, private communication; see Hofmeister et al. 2003; Speck et al. 2011 for details of laboratory procedures) and following the procedures described by Speck et al. (2011) to obtain absorption efficiencies/cross sections for comparison with astronomical data, we produced the spectrum shown in Figure 7. From inspection, we can see that the ~21 μm feature has a peak-to-continuum ratio of approximately half that for the ~10 μm feature. We also used the onedspec package in IRAF to determine the relative strengths of these features (as measured by EW) and find that the ~21 μm feature is ~70% as strong as the ~10 μm feature. If the blue-broadening was due to Si–O bonds in SiS_2 grains, then we would expect to see the ~21 μm feature in the continuum-divided spectra in Figure 2 and its strength should be most obvious in those objects with the broadest/bluest ~11 μm feature. There is no evidence for a ~21 μm feature in any of our sample objects. Increasing oxygen contamination may completely coat the SiS_2 grains, which would increase the strength of the ~10 μm feature relative to that at ~21 μm; however, the carbon-richness of our astronomical environments make this scenario unlikely. Indeed, while SiS_2 may be quickly and easily oxidized in the terrestrial laboratory, the same is much less likely in a reducing environment around a carbon star. The first reaction of SiS_2 with OH in a low-oxygen environment would make solid SiO rather than SiO_2, but this solid has its mid-IR feature shortward of 9 μm, which is not consistent with the added feature needed to explain the blue-broadening of the ~11 μm feature. The blue-broadening of the ~11 μm feature can be fitted quite nicely with a regular ~9.7 μm absorption feature like that seen in the ISM

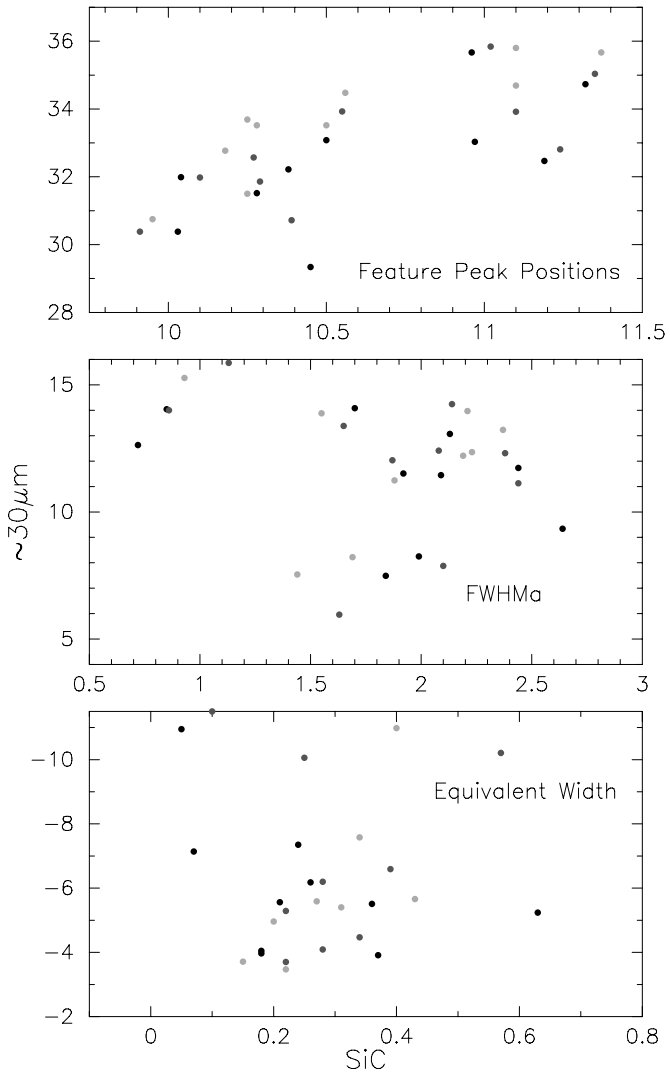

Figure 5. Relationships between the SiC and "30 μm" spectral feature parameters. In all cases, black symbols are parameters measured on spectra using blackbody continuum division; dark gray symbols are parameters measured on spectra using continuum with best-fit β-value; light gray symbols are parameters measured on spectra using continuum with $\beta = 1$. Upper panel: peak positions; middle panel: FWHMa; lower panel: equivalent widths; axes are always in μm.

(see, e.g., Speck et al. 1997; Groenewegen 1996). Speck et al. (2005) attempted to fit this feature with amorphous SiC which has a diamond-like SiC component giving a feature at ~9.3 μm, but found that this new feature is too blue to match the observed broadening.

5. IDENTIFYING THE "30 μm" FEATURE THROUGH LABORATORY DATA

As discussed in Section 1.2, many carriers have been proposed for the 30 μm feature. The most favored candidate carrier is MgS, but this remains controversial (e.g., Zhang et al. 2009a). In order to investigate some of the potential carriers of the "30 μm" feature, we analyzed the effect of composition and grain-shape distributions on potential matches to the "30 μm" feature.

Since solid particles in astrophysical environments are expected to be very irregular in shape, it is very difficult to characterize the shape of the particles in an simple way. Traditionally, cosmic dust grains have been assumed to be spherical for simplicity, however, it is becoming increasingly obvious that the use of spherical grains leads to unrealistic spectral features (see, e.g., Min et al. 2003; DePew et al. 2006; Pitman et al. 2008, 2011).

Hofmeister et al. (2003) showed that there are several sulfide minerals that could potentially match the observed "30 μm" feature. With this in mind, we have acquired the optical constants (complex refractive indices) of a range of sulfide minerals in order to test the effect of both composition and grain shape on the far-IR spectral feature. Following Min et al. (2003), we have calculated the absorption cross sections (C_{abs}) for four grain-shape distributions: spherical particles (SPH), continuous distribution of ellipsoids (CDE), continuous distribution of spheroids (CDS), and distribution of hollow spheres (DHS),[6] using the optical constants of MgS, CaS, $Mg_{0.9}Fe_{0.1}S$ (Fe10S), $Mg_{0.75}Fe_{0.25}S$ (Fe25S), $Mg_{0.5}Fe_{0.5}S$ (Fe50S), and $Mg_{0.1}Fe_{0.9}S$ (Fe90S). The optical constants for CaS and MgS came from Hofmeister et al. (2003)[7] while the Fe10S–Fe90S data came from Begemann et al. (1994).[8] For the purposes of these calculations, we assume the grains have a volume equivalent sphere radius of 0.1 μm. While the dust grains almost certainly have a range of sizes, the precise size distribution of the grains is not known. Moreover, Speck et al. (2009) discussed in great detail the issue of grains sizes in our sample stars and showed that 0.1 μm-sized grains produce identical results in radiative transfer models as do the more "realistic" distributions (e.g., Mathis et al. 1977; Kim et al. 1994).

While the calculations performed here are only valid in the Rayleigh limit, that limit is met with 0.1-μm-sized grains when looking at spectral features in the mid- and far-IR. The resulting absorption cross sections (spectra) are shown in Figure 8 (demonstrating compositional effect) and Figure 9 (demonstrating grain-shape effect). The shapes and positions of the ~30 μm features shown do not depend on short wavelength data (the optical constants are limited to $\lambda > 1\,\mu$m), but the strengths of any observed emission features to which these data are compared will depend on the UV–NIR absorption properties, which are largely unknown.

It is immediately obvious from Figures 8 and 9 that the use of spherical grains does not produce anything like the observed feature. In fact, as stated above, it is unlikely that calculations of cross sections using spherical grains are realistic (see, e.g., Min et al. 2003; DePew et al. 2006; Pitman et al. 2008; Corman 2010). Similarly, the calculated absorption cross sections for the most iron-rich composition (Fe90S) do not resemble the observed feature. Hony et al. (2002a) found evidence for FeS in the spectra of some PNe; based on the same sharp features we see in Figures 8 and 9 for Fe90S, we are confident that strongly iron-bearing sulfides will not show a broad, smooth 30 μm feature. We will not consider spherical grains or the Fe90S composition further. On the other hand, all other sulfide compositions (CaS, MgS, Fe10S, Fe25S, and Fe50S) give rise to very similar spectral features, which certainly have overlapping parameters. These results show that it may not be possible to distinguish what particular mineral and/or grain shape is causing the 30 μm feature. Indeed, it is possible that the observed 30 μm feature is made up of contributions from all these sulfide minerals.

[6] Hollow spheres are meant to simulate fluffy grains.
[7] Optical constants can be downloaded from http://galena.wustle.edu/~dustspec/idals.html
[8] Optical constants can be downloaded from http://www.astro.uni-jena.de/Laboratory/Database/databases.html

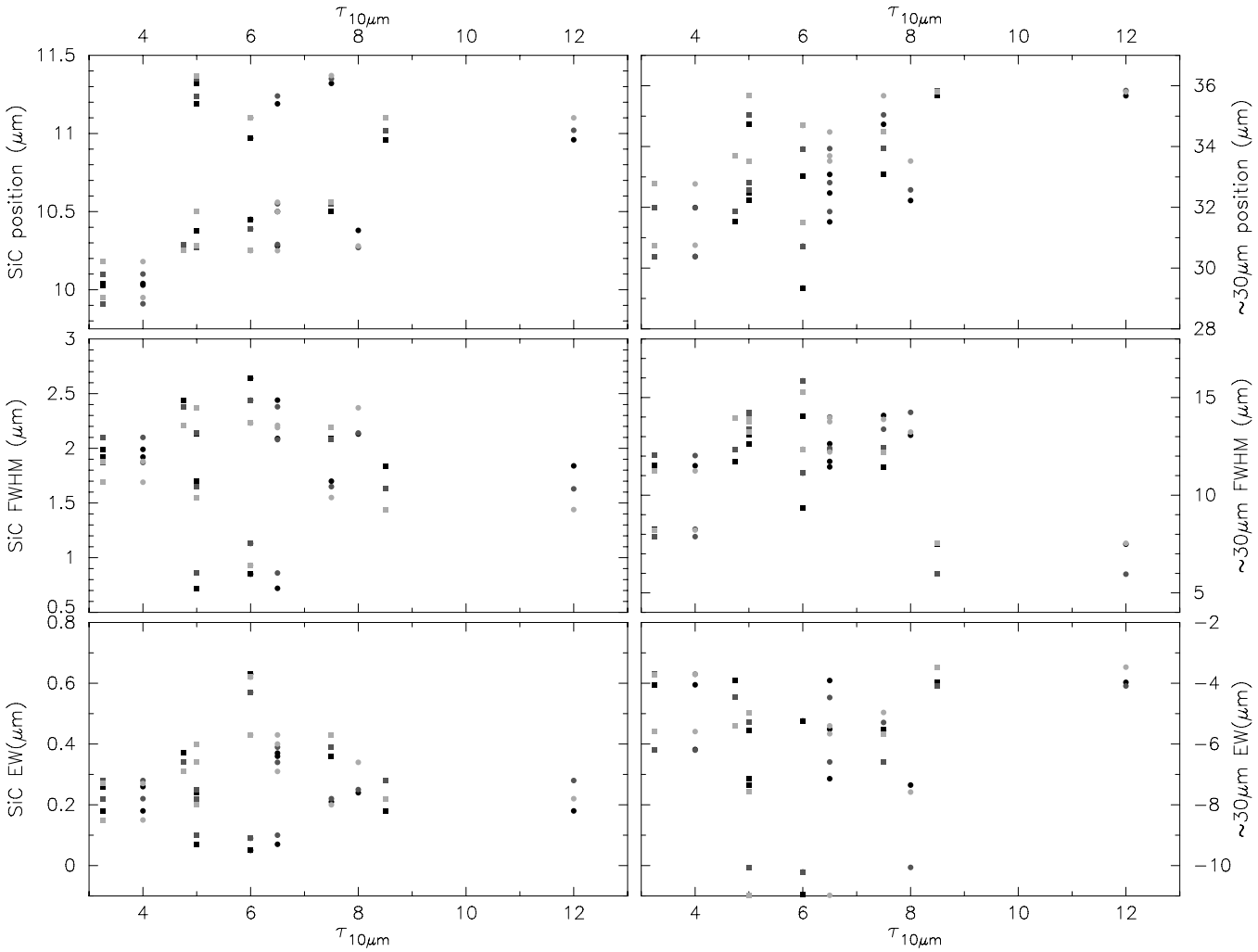

Figure 6. Relationships between modeled infrared optical depth and spectral feature parameters. In all cases, circles represent $\tau_{10\,\mu m}$ from models using the MRN grain-size distribution; triangles represent $\tau_{10\,\mu m}$ from models using the "meteoritic" grain-size distribution; black symbols represent spectral parameters measured on spectra using blackbody continuum division; dark gray symbols represent parameters measured on spectra using continuum with best-fit β-value; light gray symbols represent parameters measured on spectra using continuum with $\beta = 1$. Upper panels: peak positions; middle panels: FWHMa; lower panels: equivalent widths; left column: values for 11 μm SiC feature; right column: values for "30 μm" feature; the x-axis is always 10 μm optical depth $\tau_{10\,\mu m}$ and the y-axis is always in μm.

Zhang et al. (2009a) stated that MgS could not fulfill the necessary abundance needed to explain the 30 μm emission. They argue that the amount (by mass) of MgS dust needed to explain the 30 μm emission in HD 56126 is roughly an order of magnitude larger than that which is available, though they do recognize limitations within their analysis. Their main limitation results from the lack of viable optical constants for the UV/visible range of the MgS spectrum. In order to surmount this difficulty, they use Mie Theory and spherical grains to calculate the absorption efficiencies for this range. However, as previously discussed, spherical grains do not provide an accurate representation of the 30 μm feature and thus should not be used in any approximations, hence leading their estimates to be questionable. Adding in other minerals to explain the 30 μm feature (e.g., CaS, Fe10s, Fe25S, etc.) would only marginally increase the number of atoms contributing to the 30 μm feature. Whereas the more massive calcium and iron cations (in CaS, FeS) would seem to produce a factor of 2–3 increase in the dust mass, in fact the effect is much smaller because the carrier formation is limited by the S abundance (which is only 44% of the Mg atomic abundance). Consequently, including elements other than magnesium cannot account for an order of magnitude difference in the estimated dust mass. However, the inclusion of iron-bearing sulfides may change the UV–visible absorption properties significantly (cf. "dirty silicates"; Jones et al. 1978; Li & Li 2009; Speck et al. 2011), and thus the Zhang et al. (2009a) mass estimate may rest on underestimates for the absorptivity. Furthermore, their use of spherical grains may contribute to an underestimate of mass. Zhang et al. (2009a) appeal, as do we, for better optical constants or MgS throughout the corresponding wavelength range, which would allow us to more accurately describe potential abundance concerns. This is also true for the other sulfides considered here.

Hony et al. (2002b) analyzed various grain shapes of Fe10S and identified CDE as the most likely cause of the 30 μm feature. We acquired similar spectral feature shapes and positions for our MgS and Fe10S CDE and spherical grain emission profiles compared to those of Hony et al. (2002b). However, in our analysis we did not consider individual (aligned) grain shapes, but rather we also included the continuous distribution of spheroids. A combination of randomly oriented spheroids from Hony et al. (2002b) would look very much like our CDS profile. Hony et al. (2002b) suggested that MgS SPH grains were necessary to explain emission in some of their sources.

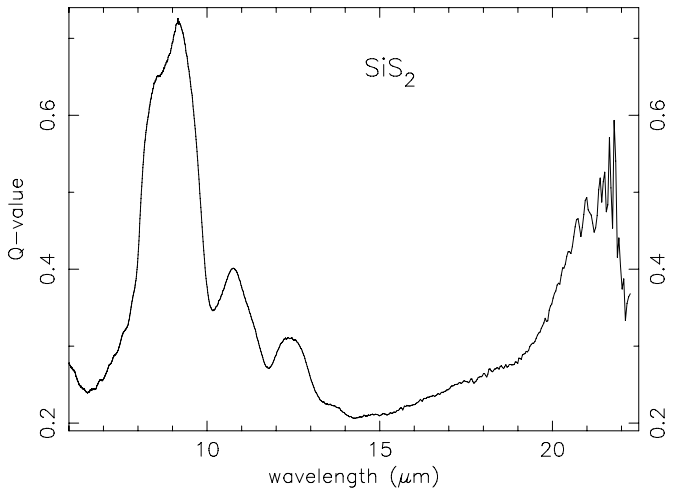

Figure 7. Absorption cross section for SiS_2: the x-axis is wavelength in μm and the y-axis is absorption efficiency Q_λ.

However, as previously discussed, SPH grains do not give rise to realistic features (regardless of the choice of mineral data) and thus this assertion of the need for spherical grains is probably erroneous.

We have extended the analysis of the 30 μm feature by including compositions other than Fe10S. We conclude that while MgS CDE can describe some observed 30 μm features, other grain shapes and compositions describe the feature equally well and the differences between profiles are not distinguishable in observational data.

6. COMPARING LAB AND OBSERVED DATA

In order to demonstrate how the laboratory mineral data compare with astronomical observations, Figure 10 shows the CDE distributions for the most disparate mineral spectra together with three exemplar astronomical sources IRAS 06582+1507, IRAS 21318+5631, and IRAS 23166+1655. IRAS 06582+1507 and IRAS 21318+5631 demonstrate the typical extreme carbon star spectra, while IRAS 23166+1655 demonstrates an extreme case in terms of the positions of both its ∼11 μm and ∼30 μm features. It is also considered an archetypal extreme carbon star (e.g., Speck et al. 2009). The CDE grain-shape distribution was chosen for comparison because it tends to exhibit an intermediate ∼30 μm spectral profile when compared to the other non-spherical grain-shape distributions (see Figures 8 and 9). By referring to these two figures, which demonstrate the effect of grain shape and composition, it is easy to see that combinations of calculated absorption cross sections can match the upper two observed astronomical spectra (i.e., IRAS 06582+1507, IRAS 21318+5631). Since these two sources are representative of the majority of other objects in our sample (see, e.g., Figure 2), the data suggest that (1) sulfides could explain the majority of observed "30 μm" features, but that (2) the precise composition of the sulfide is not measurable for this broad feature. However, the spectrum of IRAS 23166+1655 in the bottom panel of Figure 10, cannot be matched by the sulfide data presented in Section 5. The observed feature is too red to match any of the presented sulfide laboratory data. While we did not exhaust the grain-shape parameter space, it seems unlikely that we can manipulate the

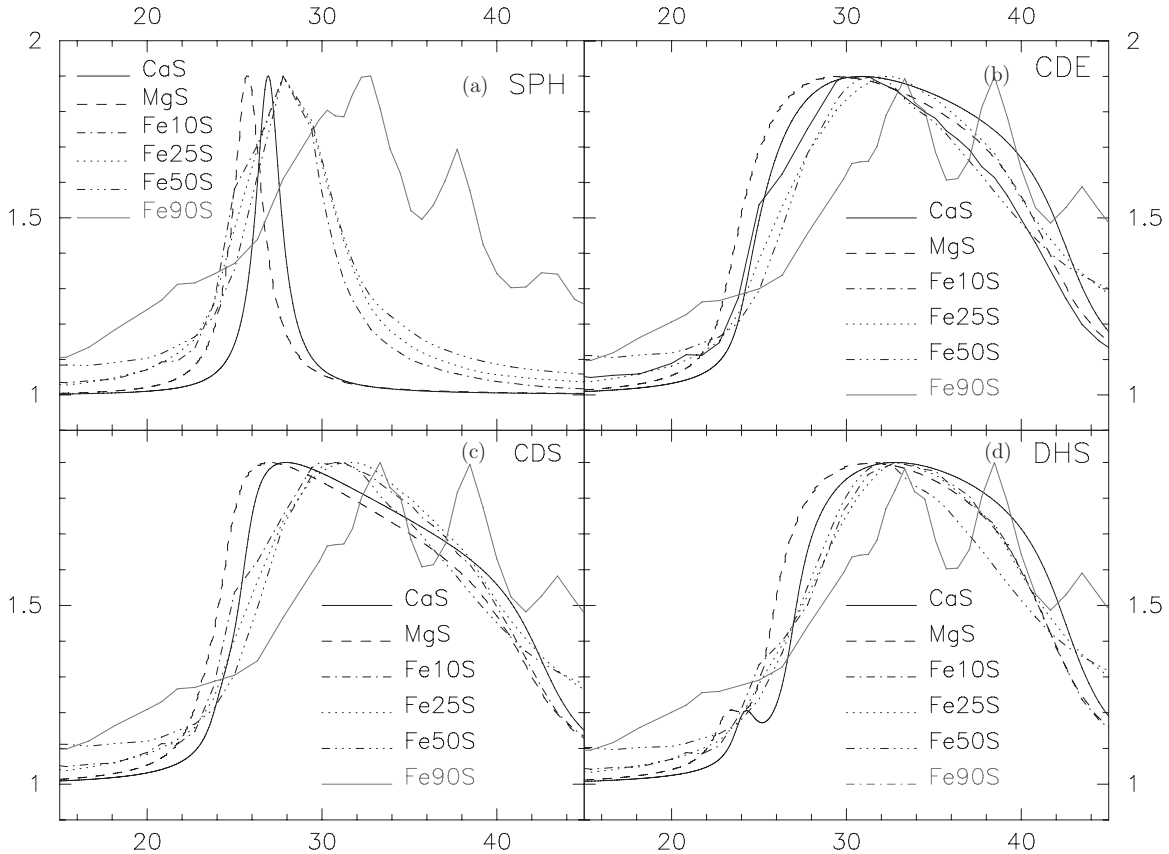

Figure 8. Effect of composition on the "30 μm" spectral feature for constant grain shape. Each panel shows the calculated absorption cross section for a different grain-shape distribution. Upper left panel: spherical grains; upper right panel: continuous distribution of ellipsoids; lower left panel: continuous distribution of spheroids; lower right panel: distribution of hollow spheres. The x-axis is wavelength in μm and the y-axis is the divided flux.

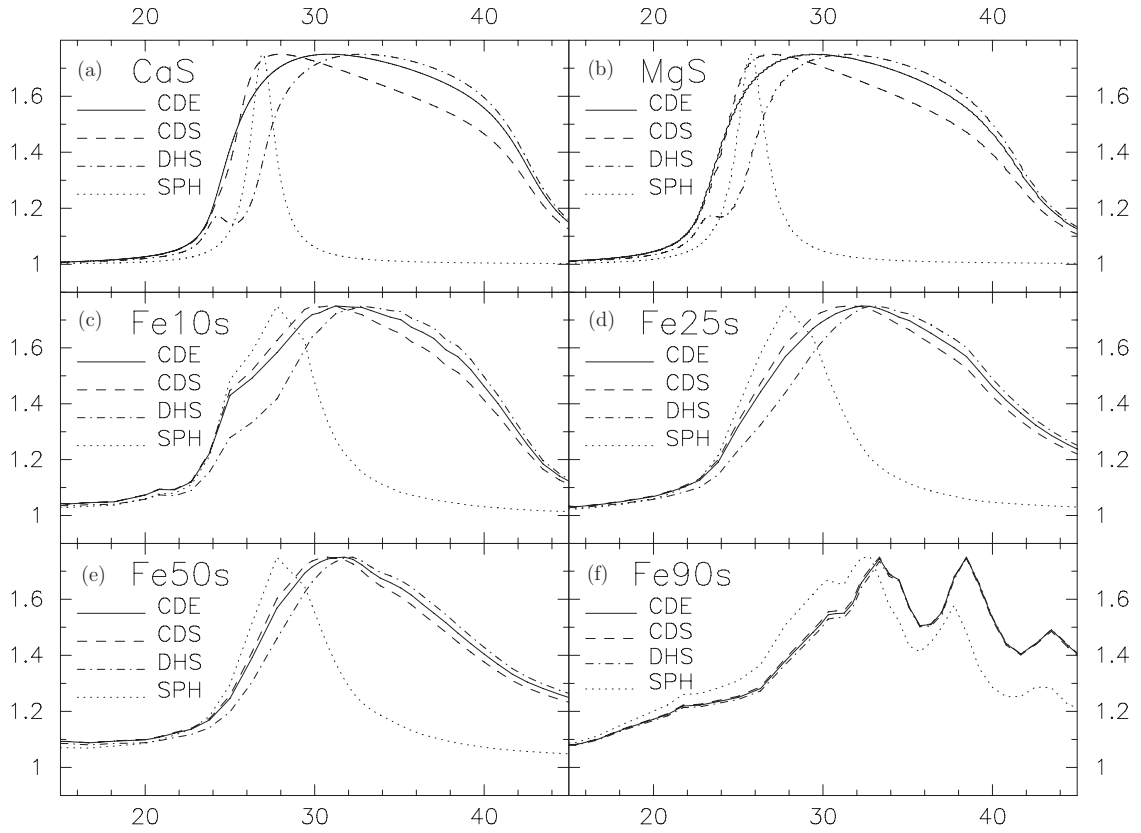

Figure 9. Effect of grain shape on the "30 μm" spectral feature for constant composition. Each panel shows the calculated absorption cross section for a different composition. SPH = spherical grains; CDE = continuous distribution of ellipsoids; CDS = continuous distribution of spheroids; DHS = distribution of hollow spheres. Upper left panel: CaS; upper right panel: MgS; middle left panel: Fe10S; middle right panel: Fe25S; lower left panel: Fe50S; lower right panel: Fe90S. The *x*-axis is wavelength in μm and the *y*-axis is the divided flux.

grain shape, size, composition, and orientation and get a match to the spectrum of IRAS 23166+1655. This strongly suggests that the identification of the "30 μm" feature solely with MgS is suspect.

7. SUMMARY, CONCLUSIONS, AND FUTURE DIRECTIONS

We have investigated the so-called 30 μm feature both in astronomical observations and in laboratory spectra of sulfide minerals. Our study reveals the following.

1. Neither perfectly spherical nor strongly iron-bearing sulfide grains can provide matches to the observational data on the "30 μm" feature in any of the extreme carbon stars in our sample.
2. Whatever species are responsible for the 30 μm feature is not coating the extant SiC grains, although we cannot rule out carbon grains as seeds for sulfide grain formation.
3. As long as we reject spherical and very-iron-rich sulfide grains, there is a range of Mg–Fe–Ca sulfides whose emission profiles are essentially indistinguishable in many cases.
4. While the majority of observational data in our sample could be explained by a combination of sulfides in a range of compositions and grain shapes, IRAS 23166+1655 (AFGL 3068) cannot be so easily explained. This object is the prototypical extreme carbon star, and the present *ISO* SWS data are high quality. This spectrum strongly suggests that sulfides in general, and MgS in particular, cannot fully describe the "30 μm" feature. We support the findings of Zhang et al. (2009a) that MgS is not sufficiently supported by the observational evidence to hold the current "best hypothesis" status.
5. Correlations between peak positions of the $\sim$11 μm and $\sim$30 μm features and with modeled optical depth of these circumstellar shells implies that the carriers are intimately linked and depend on the dust shell density. However, caution is needed when interpreting correlations, no matter how statistically significant.
6. The lack of an observable 21 μm feature in our spectra is evidence against oxidized SiS_2 as the cause of the blue-broadening of the 11 μm feature. However, it is possible that SiS_2 grains may be completely coated in SiO by reaction with OH at the grain surface. This may suppress the 21 μm feature and generate an Si–O stretching vibration. Unfortunately, the Si–O stretch for SiO is too blue to be consistent with the observed blue-broadening of the 11 μm feature. It would be interesting to investigate whether SiS_2 coated with SiO would give rise to such a blue feature or whether it would be sufficiently red to explain the blue-broadening of the 11 μm feature. Furthermore, another question that should be addressed is what fraction of SiS_2 needs to be converted to SiO or SiO_2 to sufficiently diminish the 21 μm feature. In terrestrial laboratory conditions, SiS_2 is easily oxidized to SiO_2 because oxygen is readily available. In carbon-rich cosmic environments, the C/O can vary from only just above unity to $\sim$2 with Galactic carbon stars having a mean C/O $\approx$1.15 (Lambert et al. 1986; Ohnaka et al. 2000). Post-AGB stars that exhibit the enigmatic 21 μm feature are known to be very carbon-rich

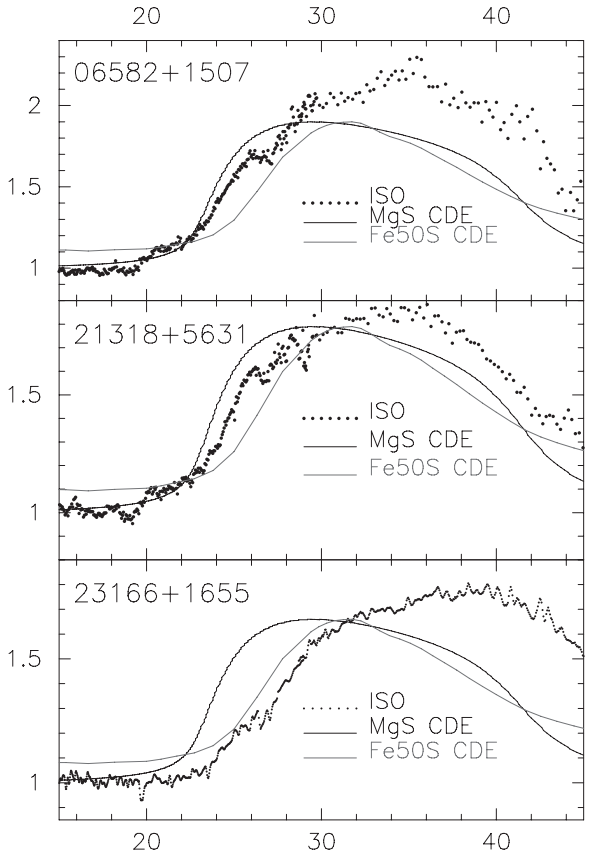

Figure 10. Three sample sources demonstrating comparison between laboratory and observational data. Only CDE grain-shape distribution and only MgS and Fe50S calculated absorption cross sections are shown. CDE represents the intermediate spectral profile shown in Figure 9, while MgS and Fe50S represent the extremes of the compositional effects seen in Figure 8. The smooth lines are the calculated absorption cross sections for laboratory sulfides and are normalized to the continuum-divided observed *ISO* spectra (dots). The *x*-axis is wavelength in μm and the *y*-axis is the divided flux.

and enriched in *s-process* elements (e.g., Van Winckel & Reyniers 2000). This fact led Speck & Hofmeister (2004) to suggest excess carbon in SiC grains as the cause of the 21 μm feature. If the 21 μm feature can be attributed to SiS_2, then perhaps this sulfide needs highly reducing environments, and is destroyed via oxidation in lower C/O (but still C-rich) environments. In this case, the blue-broadening in the 11 μm feature could be attributed to SiO or SiO_2 that forms on the surface of SiS_2 grains, creating a $\sim$9.5 μm feature and suppressing that at 21 μm. Clearly a laboratory study of oxidation of silicon disulfide is needed.

This work is supported in part by NSF AST-0607341. We thank Catharinus Dijkstra for his code to calculate absorption cross sections for different grain shapes of various materials, and Anne Hofmeister for her SiS_2 absorbance data. We thank Joseph Nuth for insightful comments that improved this manuscript.

REFERENCES

Baron, Y., de Muizon, M., Papoular, R., & Pégourié, B. 1987, A&A, 186, 271
Begemann, B., Dorschner, J., Henning, T., & Mutschke, H. 1996, ApJL, 464, L195
Begemann, B., Dorschner, J., Henning, T., Mutschke, H., & Thamm, E. 1994, ApJL, 423, L71
Bernatowicz, T. J., Croat, T. K., & Daulton, T. L. 2006, in Meteorites and the Early Solar System II, ed. D. S. Lauretta & H. Y. McSween, Jr. (Tucson, AZ: Univ. Arizona Press), 109
Brockett, P., & Levine, A. 1984, Statistics and Probability and Their Applications (New York: CBS College Publishing)
Chan, S. J., & Kwok, S. 1990, A&A, 237, 354
Clément, D., Mutschke, H., Klein, R., & Henning, T. 2005, ApJ, 621, 985
Cohen, M. 1984, MNRAS, 206, 137
Corman, A. B. 2010, PhD thesis, Univ. Missouri
de Graauw, T., Haser, L. N., Beintema, D. A., et al. 1996, A&A, 315, 49
DePew, K., Speck, A., & Dijkstra, C. 2006, ApJ, 640, 971
Dijkstra, C., Speck, A. K., Reid, R. B., & Abraham, P. 2005, ApJL, 633, L133
Donnelly, R. A., Jr. 2004, The Complete Idiot's Guide to Statistics (New York: Penguin Group)
Forrest, W. J., Houck, J. R., & McCarthy, J. F. 1981, ApJ, 248, 195
Friedman, C. 1969, Physica, 41, 189
Gilman, R. C. 1969, ApJL, 155, L185
Gilra, D. P., & Code, A. D. 1971, BAAS, 3, 379
Goebel, J. H., Cheeseman, P., & Gerbault, F. 1995, ApJ, 449, 246
Goebel, J. H., & Moseley, S. H. 1985, ApJL, 290, L35
Greenberg, J. M., & Chlewicki, G. 1983, ApJ, 272, 563
Groenewegen, M. A. T. 1996, A&A, 305, 475
Gruendl, R. A., Chu, Y.-H., Seale, J. P., et al. 2008, ApJL, 688, L9
Guha-Niyogi, S., Speck, A., & Takashi, O. 2011, ApJ, 733, 93
Hackwell, J. A. 1972, A&A, 21, 239
Hofmeister, A. M., Keppel, E., & Speck, A. K. 2003, MNRAS, 345, 16
Hony, S., & Bouwman, J. 2004, A&A, 413, 981
Hony, S., Bouwman, J., Keller, L. P., & Waters, L. B. F. M. 2002a, A&A, 393, L103
Hony, S., Waters, L. B. F. M., & Tielens, A. G. G. M. 2002b, A&A, 390, 533
Hrivnak, B. J., Volk, K., & Kwok, S. 2009, ApJ, 694, 1147
Iben, I., Jr., & Renzini, A. 1983, ARA&A, 21, 271
Jones, B., Merrill, K. M., Puetter, R. C., & Willner, S. P. 1978, AJ, 83, 1437
Jørgensen, U. G., Hron, J., & Loidl, R. 2000, A&A, 356, 253
Kim, S.-H., Martin, P. G., & Hendry, P. D. 1994, ApJ, 422, 164
Knapp, G. R., & Morris, M. 1985, ApJ, 292, 640
Knapp, G. R., Sandell, G., & Robson, E. I. 1993, ApJ, 88, 173
Koike, C., Hasegawa, H., & Hattori, T. 1987, Ap&SS, 134, 95
Koike, C., Hasegawa, H., & Manabe, A. 1980, Ap&SS, 67, 495
Koike, C., Kimura, S., & Kaito, C. 1995, ApJ, 446, 902
Kraus, G. F., Nuth, J. A., & Nelson, R. N. 1997, A&A, 328, 419
Lambert, D. L., Gustafsson, B., Eriksson, K., & Hinkle, K. H. 1986, ApJS, 62, 373
Le Bertre, T. 1987, A&A, 176, 107
Leech, K., Kester, D., Shipman, R., et al. 2003, in The ISO Handbook, Vol. V. SWS—The Short Wavelength Spectrometer Version 2.0.1 (2003 June), series, ed. T. G. Mueller, J. A. D. L. Blommaert, & P. Garcia-Lario (ESA SP-1262; Noordwijk: ESA)
Leisenring, J. M., Kemper, F., & Sloan, G. C. 2008, ApJ, 681, 1557
Li, M. P., & Li, A. 2009, Aigen Am. Astron. Soc., AAS Meeting, 214, 402.20
Lodders, K., & Fegley, B. 1995, Metic, 30, 661
Mathis, J. S., Rumpl, W., & Nordsieck, K. H. 1977, ApJ, 217, 425
Mennella, V., Colangeli, L., & Bussoletti, E. 1998, ApJ, 496, 1058
Messerli, F. H. 2012, New Engl. J. Med., 367, 1562
Min, M., Hovenier, J. W., & de Koter, A. 2003, A&A, 404, 35
Nuth, J. A., Moseley, S. H., Silverberg, R. F., Goebel, J. H., & Moore, W. J. 1985, ApJL, 290, L41
Ohnaka, K., Tsuji, T., & Aoki, W. 2000, A&A, 353, 528
Olnon, F. M., Raimond, E., Neugebauer, G., et al. 1986, A&AS, 65, 607
Omont, A., Moseley, S. H., Cox, P., et al. 1995, ApJ, 454, 819
Pitman, K. M., Hofmeister, A. M., Corman, A. B., & Speck, A. K. 2008, A&A, 483, 661
Pitman, K. M., Speck, A. K., & Hofmeister, A. M. 2006, MNRAS, 371, 1744
Pitman, K. M., Speck, A. K., Hofmeister, A. M., & Corman, A. B. 2011, in Silicon Carbide—Materials, Processing and Applications in Electronic Devices, ed. M. Mukherjee (New York: InTech Open Acess Publishing)
Renzini, A. 1981, in Physical Processes in Red Giants, ed. I. Iben, Jr. & A. Renzini (Reidel: Dordrecht), 431
Rouleau, F., & Martin, P. G. 1991, ApJ, 377, 526
Rumsey, D. 2003, Statistics for Dummies (New York: Wiley)
Sloan, G. C., Little-Marenin, I. R., & Price, S. D. 1998, AJ, 115, 809
Speck, A. K., Barlow, M. J., & Skinner, C. J. 1997, MNRAS, 288, 431
Speck, A. K., Cami, J., Markwick-Kemper, C., et al. 2006, ApJ, 650, 892
Speck, A. K., & Hofmeister, A. M. 2004, ApJ, 600, 986
Speck, A. K., Thompson, G. D., & Hofmeister, A. M. 2005, ApJ, 634, 426
Speck, A. K., Corman, A. B., Wakeman, K., et al. 2009, ApJ, 691, 1202
Speck, A. K., Whittington, A. G., & Hofmeister, A. M. 2011, ApJ, 740, 93

Szczerba, R., Henning, T., Volk, K., Kwok, S., & Cox, P. 1999, A&A, 345, L39
Thompson, G. D., Corman, A. B., Speck, A. K., & Dijkstra, C. 2006, ApJ, 652, 1654
Treffers, R., & Cohen, M. 1974, ApJ, 188, 545
Van Winckel, H., & Reyniers, M. 2000, A&A, 354, 135
Vassiliadis, E., & Wood, P. R. 1993, ApJ, 413, 641
Villaver, E., Manchado, A., & Garcia-Segura, G. 2002a, ApJ, 581, 1204
Volk, K., Kwok, S., Hrivnak, B. J., & Szczerba, R. 2002, ApJ, 567, 412
Volk, K., Kwok, S., & Langill, P. 1992, ApJ, 391, 285
Willems, F. J. 1988, A&A, 203, 51
Wood, P. R., Whiteoak, J. B., Hughes, S. M. G., et al. 1992, ApJ, 397, 552
Xiang, Y., Li, A., & Zhong, J. X. 2011, ApJ, 733, 91
Zhang, K., Jiang, B. W., & Li, A. 2009a, ApJ, 702, 680
Zhang, K., Jiang, B. W., & Li, A. 2009b, MNRAS, 396, 1247
Zhukovska, S., & Gail, H.-P. 2008, A&A, 486, 229
Zijlstra, A., Matsuura, M., Wood, P. R., et al. 2006, MNRAS, 370, 1961